Available online at www.sciencedirect.com
SCIENCE DIRECT®
Journal of Catalysis 221 (2004) 191–203
JOURNAL OF CATALYSIS
www.elsevier.com/locate/jcat

Support and rhenium effects on the intrinsic site activity and methane selectivity of cobalt Fischer–Tropsch catalysts

Christopher J. Bertole,[a] Charles A. Mims,[a] and Gabor Kiss [b,*]

[a] *Department of Chemical Engineering and Applied Chemistry, University of Toronto, Toronto, ON M5S3E5, Canada*
[b] *ExxonMobil Research and Engineering Company, Corporate Strategic Research Laboratories, 1545 Route 22 East, Annandale, NJ 08801, USA*

Received 16 May 2003; revised 4 August 2003; accepted 5 August 2003

Abstract

Catalyst composition effects on site activity, active carbon coverage, and methane selectivity in the cobalt-catalyzed Fischer–Tropsch synthesis were examined using $^{12}CO \rightarrow {}^{13}CO$ isotope transients at reaction steady state. All catalysts (18 total) were tested at identical conditions: 221 °C, 6.5 atm of $H_2/CO/Ne = 2/1/1$. The intrinsic site activity of unsupported Co and Co-supported on SiO_2, TiO_2, and Al_2O_3 (Co dispersion $< 10\%$) varies within a relatively narrow band ($\sim 2x$ maximum rate difference). Re present at a Re/Co weight ratio of 0.1 does not affect Fischer–Tropsch activity and selectivity. Since its own activity is 20 times lower than that of Co, Re does not appear to block or modify active Co sites. While Re and the above-noted three common oxide supports do not affect the Fischer–Tropsch activity and selectivity of the relatively large cobalt crystallites, some modifications of SiO_2 and Al_2O_3 supports (with MgO, Y_2O_3, ZnO, and Ce_2O_3, by coating and coprecipitation) reduce site activity by up to an order of magnitude. Interestingly, the reduced site activity does not measurably affect methane selectivity. For all catalysts, the observed site-activity differences, whether small or large, do not correlate with bulk composition, and are possibly the result of unidentified impurities introduced during catalyst preparation. These impurities affect the reactivity of both the adsorbed CO and the active carbon present on the catalyst: higher site activity correlates with higher active carbon reactivity. Although this correlation is strong, some variability in the CO/C^* reactivity ratio does occur. This variability appears to play a key role in methane selectivity, namely, higher values correlate with lower methane selectivity. These observations can be rationalized by our previously published simple kinetic model.

Keywords: Fischer–Tropsch synthesis; Cobalt catalyst; Rhenium promoter; Active carbon inventory and reactivity; Methane selectivity; Site activity; Support and promoter effect; Isotope transient

1. Introduction

Cobalt-catalyzed Fischer–Tropsch (FT) synthesis, the conversion of syngas (H_2 and CO) into hydrocarbons and water, is generally considered a structurally insensitive reaction. Iglesia and co-workers [1–6], for example, found that under conditions favoring chain growth (as opposed to methanation), CO turnover frequency was unaffected by varying the cobalt metal crystallite size between 10 and 210 nm. The lack of support and metal promoter effects was also notable. Overall, their reported site-activity values were within a factor of 2. Several others have obtained similar results under methanating conditions [7–9]. In a more recent study [10], Oukaci et al. compared the activity and selectivity of eight TiO_2-, SiO_2-, and Al_2O_3-supported catalysts with or without metal and/or oxide promoters. They concluded that while the support and the promoter influenced catalyst properties, the turnover frequencies were within the combined experimental error of the chemisorption and activity measurements. Similarly, Holmen's group has reported [11,12] that zirconia modification of alumina and/or noble metal promotion did not change the intrinsic activity of supported cobalt catalysts. These results may relate to the finding that crystallite surface structure and orientation are little influenced by crystallite size for diameters greater than 10 nm [6], which corresponds to a Co dispersion of approximately 10%.

Most of the above-cited studies used ex situ methods, such as hydrogen chemisorption, for quantifying the number of active sites. These ex situ methods, of course, cannot account for changes in site density that may occur due

* Corresponding author.
E-mail address: gabor.kiss@exxonmobil.com (G. Kiss).

0021-9517/$ – see front matter
doi:10.1016/j.jcat.2003.08.006

to possible deactivation, which is a concern in the cobalt-catalyzed FT synthesis. It is known, for example, that the water by-product can reduce catalytic activity, even in the absence of any extrinsic poisons [13, and references therein]. This in situ deactivation is the likely reason for the apparent changes in intrinsic activity reported by Barbier et al. [14] for their silica-supported Co catalysts. They found that site activity increased up to a critical cobalt particle diameter of ~ 6 nm, above which it was constant. As they suggested in their paper, this apparent change was likely due to the instability of small Co particles in the FT synthesis. While they did use cobalt crystallite sizes measured postreaction to calculate site activity, which at least accounted for deactivation due to sintering, it is unclear if cobalt silicate formation also reduced the number of active sites, and if so, whether they accounted for it in their calculations. Clearly, site activity would be better characterized by using an in situ site-counting method.

While the lack of support and promoter effects for the typical, relatively low dispersion cobalt FT catalyst has been reasonably established, the effect of support and metal promoters on methane and C_{5+} selectivity remains controversial. Iglesia, for example, found the same methane selectivity with SiO_2-, TiO_2-, and Al_2O_3-supported catalysts with similar intraparticle transport/site-density characteristics [1], but others reported significant support [10] and metal promoter effects [15]. In our own experience, methane selectivity is very sensitive to reaction conditions, CO conversion, and possible mass transfer limitations. Therefore, establishing the intrinsic effects of support and promoters is difficult and requires strict control of reaction conditions and the careful elimination of mass transfer limitations.

In light of the above discussion and to further advance our understanding of the effects of support and metal promoters on catalytic activity and selectivity in the FT synthesis, the current study has the following objectives:

1. Determine the effect of support, support modification, and Re promoter on the intrinsic site activity of cobalt catalysts by using in situ counted active sites, thus eliminating potential errors from deactivation loss during FT synthesis.
2. Determine the effect of support, support modification, and Re promoter on the intrinsic methane selectivity of cobalt in the absence of process variable and mass-transport effects.
3. Determine the adsorbed CO and active carbon inventories and their reactivities and investigate their correlation with changes in site activity and selectivity.

The reported investigation involved 18 catalyst samples with various supports (commercially available SiO_2, TiO_2, Al_2O_3, and modified supports) and Co loadings (5–30 wt%), both with and without Re (Re/Co = 0.02–0.03 mole ratio for Co–Re catalysts). All catalysts were tested at identical conditions, 221 °C, 6.5 atm of $H_2/CO/Ne = 2/1/1$, to ensure valid comparisons between the different catalyst groups.

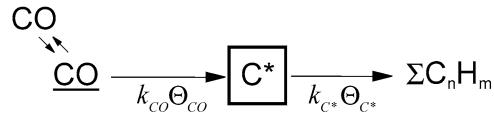

Fig. 1. Simple kinetic model of CO conversion in Fischer–Tropsch synthesis [13].

For the in situ interrogation of the catalytic process, we used $^{12}CO \rightarrow {}^{13}CO$ isotope transients at reaction steady state at elevated pressure, which favors chain growth, an industrially important objective. The carbon isotope transients measured the inventory of reversibly adsorbed CO (N_{CO}), the amount of active carbon surface intermediates (N_{C^*}), and their respective reactivities, k_{CO} and k_{C^*}. As we discussed in our earlier paper [13] on the effect of water in Co-catalyzed FT synthesis, we used N_{CO} to quantify the number of active sites, N_S, by assuming that $N_S = N_{CO}$. We need to emphasize that this site-counting method is not absolute, but is valid as long as the true number of active sites is proportional to N_{CO}. We cannot prove that this assumption is correct; however, all other site-counting methods rely on the same assumption. Using a site count obtained under reaction conditions should improve on ex situ obtained values, since it eliminates the potential error due to site losses during reaction and postreaction handling. For the data analysis and interpretation, we relied on a simple kinetic model (see Fig. 1) that was described in detail in Ref. [13]. One of the important consequences of the kinetic model in Fig. 1 is that at steady state, the active carbon coverage (Θ_{C^*}) is determined by a dynamic balance between CO activation to form C^* and the sequential reaction of C^* to form hydrocarbons:

$$k_{CO}\Theta_{CO} = k_{C^*}\Theta_{C^*}. \quad (1)$$

2. Experimental

2.1. Experimental apparatus

FT synthesis reactions were performed in a single pass, downflow, tubular (4 mm i.d.), quartz, fixed-bed microreactor. The reactor, a modified version of that described by Mauti [16], is shown schematically in Fig. 2. The quartz reactor tube was held concentrically inside a stainless-steel tube which served as the pressure vessel. Quartz wool was packed loosely inside the quartz reactor tube to support the catalyst charge. Additional quartz wool was packed on top of the catalyst bed to protect it against back surges. A K-type thermocouple, placed directly into the middle of the catalyst bed, monitored the reaction temperature, which was controlled by a second thermocouple embedded in the furnace refractory wall. Pressure control in the reactor was achieved by using a backpressure regulator. An argon purge stream of 40 ml/min (STP) flowed through the annulus between

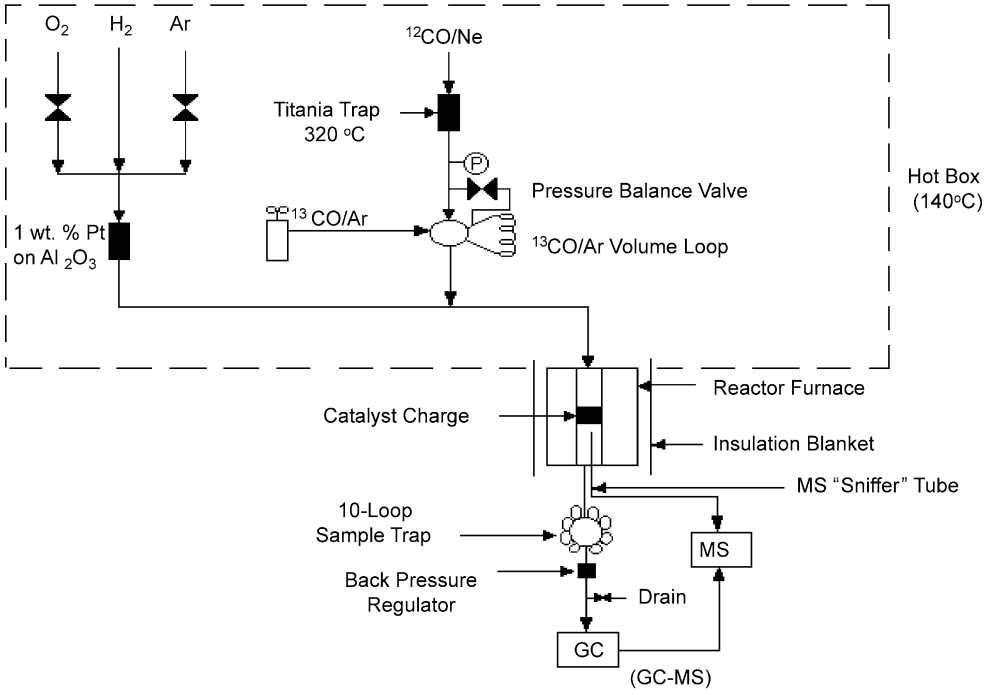

Fig. 2. Main components of the transient kinetic unit (Unit T).

the stainless-steel housing and the quartz reactor tube. It mixed with the reactor effluent at the bottom of the reactor tube, reducing holdup, downstream residence time, and condensation in the GC sampling lines. Blank experiments (TiO_2 diluent only, reduced at 375 °C in atmospheric H_2) showed no activity for CO conversion and methane production between 220 and 290 °C. Isotope transients in the blank experiments indicated that the reactor system and diluent (titania support) had no CO holdup. Blank experiments with unreduced catalysts also showed no CO adsorption, verifying that the adsorbed CO measured in catalytic runs with reduced catalysts was actually adsorbed on the active catalytic metal.

The reactor effluent was analyzed using two methods, mass spectrometry (MS) and gas chromatography (GC). A differentially pumped quartz capillary leak (3 mm o.d.) situated directly under the catalyst bed allowing continuous monitoring of the reactor effluent by on-line MS (Model UTI100C). The MS had a pinhole opening sized for ~ 1 ml/min (STP) of flow with a pressure gradient of 6.5 atm. A roughing pump maintained a pressure of $\sim 10^{-2}$ Torr in the sampling lines. Gas flow from this differentially pumped region into the MS chamber occurred through a Varian leak valve. The Varian Vacion pump and a Seiko STP300 turbomolecular pump provided an idle chamber pressure of 10^{-9} Torr.

A Hewlett Packard HP5880A gas chromatograph was used for the GC-MS analysis in the kinetic measurements. It was equipped with an 8-foot column filled with Porapak Q and S packing material (80:20 mix ratio) and a flame ionization detector (FID). Injections were made into the column using a 2-way, 6-port Valco valve that contained a 1-ml sample loop. This valve was located downstream of the backpressure regulator and thus operated at atmospheric pressure. A differentially pumped stainless-steel capillary tube (0.1 mm i.d.) placed on a tee directly at the outlet of the GC column allowed for simultaneous GC-MS analyses of the non-FID-sensitive compounds (i.e., CO, Ne, H_2, and CO_2). Product characterization using this particular GC setup was limited, allowing the quantification of only the C1–C4 hydrocarbons.

In the isotope transient experiments, we used the "volume-loop" method to switch between the ^{12}CO/Ne and ^{13}CO/Ar feeds instead of the more conventional two-feed stream method. Thus, a volume loop was installed on the ^{12}CO/Ne line (Fig. 2) to hold a plug of ^{13}CO/Ar gas, which could be inserted into the reactor feed (replacing ^{12}CO/Ne) during steady-state operation to start the isotope transient experiment. As the inserted plug passed through the reactor, the resulting forward and reverse isotope transients were recorded. This method greatly simplified the isotope transients compared to the two-feed stream method, since it facilitated easy pressure balancing between the filled loop and the reactor feed lines.

Two experiments reported in the current study were also performed using a newer transient reactor (Unit C) capable of operating at higher pressures (up to 28 bar). This unit was described in a previous publication [13]. Except for the reactor, its principal design is similar to Unit T shown in Fig. 2, and thus will not be detailed here. Notable equipment

differences include the on-line mass spectrometer (Balzers QMS420) and the on-line gas chromatograph (HP5890 with flame ionization detector and 60 m Supelco SPB-1 capillary column).

2.2. Catalysts

In order to determine the effect of support and rhenium promoter on site activity and selectivity in cobalt-catalyzed FT synthesis, we tested 18 catalyst samples. Of the 18 samples, one was unsupported cobalt (catalyst 1), four were cobalt-only catalysts (samples 2–5), 12 contained rhenium-promoted cobalt (catalysts 6–17), and one was titania-supported Re (18). The supports included unmodified silica, alumina or titania, yttria-, magnesia-, or ZnO-modified silica, alumina, or silica-alumina, and coprecipitated ceria-magnesia. The diversity of the selected supports was intended to yield some general conclusions regarding support effects. With regards to the metal promoter, we chose Re because of its known effectiveness as a cobalt dispersion and reduction aid [17]. Our current study on the effects of Re complements a series of other recent studies on the effects of metal reduction promoters in cobalt-catalyzed FT synthesis [17–29].

All catalysts were prepared using well-known techniques [1–6,10,17,30–32]. Table 1 lists the composition of each tested catalyst sample. Almost all catalysts were used with a particle size sieved below 75 μm (200 mesh) in order to avoid intraparticle mass-transfer limitations (see Table 2). There were only a few exceptions where the catalyst particle size was substantially greater than 75 μm. In these instances, mass-transfer limitations were unlikely, due to either the morphology (experiment 1 with Co powder) or the low activity (experiment 2 with Co/SiO_2 and experiment 27 with Re/TiO_2) of the catalyst. In the tables and in the text, we use the following catalyst label convention: {support identity}-{Co wt%}-{Re wt%}-{aliquot number}, e.g., Si-Co20-Re1.7-1 represents SiO_2 support, 20 wt% Co, 1.7 wt% Re, and aliquot number = 1. Other support abbreviations include Ti = TiO_2, Al = Al_2O_3, YAl = $Y_2O_3 \cdot Al_2O_3$, YSiAl = $Y_2O_3 \cdot SiO_2 \cdot Al_2O_3$, ZnSiAl = $ZnO \cdot SiO_2 \cdot Al_2O_3$, MgSi = $MgO \cdot SiO_2$, and CeMg = $Ce_2O_3 \cdot MgO$. Where catalyst samples have an aliquot number > 1, multiple experiments were performed using the same catalyst batch, each time with a new aliquot. Metal loading for the supported catalysts is given for the fully calcined state, in which the Co and Re are present as Co_3O_4 and Re_2O_7, respectively. The cobalt content ranges from 6 to 30 wt% for the supported catalysts. The Re content in the Co–Re samples is approximately 1/10 by weight of the cobalt loading corresponding to 2–3 mol%. Cobalt metal dispersions (N_{CO}/N_{Co}) for all catalysts range from 0.1 to 7.9%, as deduced from the in situ CO inventories measured in the isotope transient experiments. Particle sizes obtained by transmission electron microscopy invariably yielded higher dispersion values than obtained by in situ CO titration indicating a lower than 1:1 stoichiometry for CO adsorption.

2.3. Gases

The gases used in the experiments were H_2 (Grade 5.0, BOC), ^{12}CO/Ne (50% CO and 50% Ne custom blend, Matheson), ^{13}CO/Ar (50% ^{13}CO and 50% Ar, UHP, with the ^{13}CO from Isotec, 99% ^{13}C, 10% ^{18}O), Ar (Matheson, UHP), and air (Canox). All gases were used without further purification, except for the ^{12}CO/Ne, which was passed through a 320 °C carbonyl trap filled with 60–150 mesh TiO_2.

Table 1
Catalyst compositions

Catalyst		Support	Metal loading (wt%)	
No.	Label		Co	Re
1	Co-powder	None	100.0	0.0
2	Si-Co21	Precipitated silica	20.9	0.0
3	Ti-Co6	Rutile titania	5.7	0.0
4	Ti-Co14	Rutile titania	14.5	0.0
5	CeMg-Co18	Coprecipitated ceria–magnesia	18.4	0.0
6	Si-Co10-Re0.8	EH5 fumed silica (Cabot)	10.3	0.8
7	Si-Co20-Re1.7	EH5 fumed silica (Cabot)	19.7	1.7
8	Si-Co30-Re2.5	EH5 fumed silica (Cabot)	30.4	2.5
9	Ti-Co11-Re0.9	Rutile titania	11.3	0.9
10	Ti-Co12-Re1.2	Rutile titania	11.9	1.2
11	Ti-Co18-Re0.6	Rutile titania	17.9	0.6
12	Al-Co12-Re1.0	Alumina	12.0	1.0
13	Al-Co20-Re2.2	Alumina	20.3	2.2
14	YAl-Co20-Re1.4	15 wt% yttria on alumina	20.2	1.4
15	YSiAl-Co36-Re3.0	20 wt% yttria on silica–alumina	36.0	3.0
16	ZnSiAl-Co36-Re3.0	15.3 wt% ZnO on silica–alumina	36.0	3.0
17	MgSi-Co36-Re3.0	8.2 wt% magnesia on silica	36.0	3.0
18	Ti-Re2.8	Rutile titania	0.0	2.8

Table 2
Catalyst charges and reduction conditions

Exp.	Catalyst			Diluent[a]	Initial catalyst reduction[b]
No.	Sample	(μm)	(g)	(g)	Hold time/temperature (min/°C)
1	Co-powder-1	< 200	0.487	0.000	420/375
2	Si-Co21-1	200–400	0.122	0.102	65/375
3	Ti-Co6-1	< 75	0.109	0.100	70/374
4	Ti-Co6-2	< 75	0.200	0.080	118/370
5	Ti-Co14-1	< 75	0.160	0.154	106/390
6	CeMg-Co18-2	< 75	0.473	0.000	317/381
7	Si-Co10-Re0.8-2	< 75	0.030	0.000	65/379
8	Si-Co20-Re1.7-1	< 75	0.040	0.100	93/375
9	Si-Co30-Re2.5-1	< 75	0.040	0.103	71/376
10	Si-Co30-Re2.5-2	< 75	0.040	0.104	60/376 then 152/450
11	Si-Co30-Re2.5-3	< 75	0.040	0.104	68/377
12	Ti-Co11-Re0.9-1	< 75	0.149	0.149	90/375
13	Ti-Co12-Re1.2-1	< 75	0.200	0.100	70/374
14	Ti-Co18-Re0.6-1	< 75	0.080	0.109	75/375
15	Al-Co12-Re1.0-2	< 75	0.097	0.101	69/376
16	Al-Co12-Re1.0-3	< 75	0.097	0.104	69/376 then 60/450
17	Al-Co20-Re2.2-3	< 75	0.090	0.102	65/378
18	Al-Co20-Re2.2-4	< 75	0.090	0.102	65/376 then 56/452
19	YAl-Co20-Re1.4-2	< 75	0.118	0.111	66/376 then 74/450
20	YSiAl-Co36-Re3.0-1	< 75	0.040	0.101	70/376
21	YSiAl-Co36-Re3.0-2	< 75	0.040	0.101	72/377 then 35/451
22	ZnSiAl-Co36-Re3.0-1	< 75	0.041	0.101	79/378 then 112/450
23	ZnSiAl-Co36-Re3.0-2	< 75	0.040	0.101	79/376
24	ZnSiAl-Co36-Re3.0-3	< 75	0.103	0.151	77/377
25	MgSi-Co36-Re3.0-2	< 75	0.059	0.102	70/376
26	MgSi-Co36-Re3.0-3	< 75	0.059	0.103	70/377 then 50/450
27	Ti-Re2.8-1	< 150	0.198	0.000	52/375
28	Ti-Co11-Re0.9-2	< 75	0.150	0.181	60/400
29	Al-Co20-Re2.2-5	< 100	0.085	0.341	60/450

[a] TiO_2, 60–150 mesh.
[b] In 40 ml/min atmospheric H_2.

2.4. Experimental procedure

The catalyst charge (20–500 mg), mixed with diluent (TiO_2, 0–150 mg, 60–150 mesh) to help maintain isothermal conditions during the FT reaction, was loaded into the reactor (the exact catalyst and diluent charges are listed in Table 2). Before the catalytic tests, the catalyst was reduced in 1 atm H_2 flowing at 40 ml/min. The typical pressure drop across the catalyst bed at ambient pressure was ∼0.1 atm. During reduction, the temperature was ramped from ambient to the final reduction temperature at 0.5 °C/min (for the detailed reduction conditions see Table 2). After reduction, the catalyst was cooled to 190–200 °C in H_2. Once the catalyst bed was cooled below 200 °C, the reactor feed was switched to syngas ($H_2/CO/Ne = 2/1/1$), and the pressure and temperature were gradually raised to 5.5 atm (gauge) and 221 °C, respectively. All catalysts were tested under a single, constant set of conditions: 221 °C, $P_{total} = 6.5$ atm (absolute), $H_2/CO/Ne = 2/1/1$. The gas hourly space velocity (GHSV) was adjusted to maintain $12 \pm 4\%$ CO conversion (see Table 3). Although in most experiments we were able to meet this target, in some case catalyst activity was too low to reach the target conversion range. This careful control of reaction conditions was vital for valid comparisons to separate effects of the catalyst and the reaction conditions on the measured performance, particularly on methane selectivity. The reported activity values were obtained after ∼16–20 h on stream to allow sufficient time for the catalyst pores to fill with liquid products.

In the kinetic analyses of the data, we assumed differential conditions, an assumption justified by the low CO conversion levels. Although some FT products, e.g., water, affect the reaction kinetics [1–6,13], maintaining a narrow range of CO conversion in all of the experiments should make any effects of indigenous H_2O on the isotope and rate bed profiles similar for all tested catalysts. This, in turn, should allow a valid comparison of activity and selectivity data.

After verifying steady-state operation (6–8 mass balances over the span of 2–4 h), the isotope transients were performed. The volume loop (see Fig. 2) was first evacuated using a roughing pump, and then filled to the appropriate pressure with $^{13}CO/Ar$ gas (1/1 mixture). Pressures between the volume loop and the reactor were balanced by using a line that connected the volume loop with the $^{12}CO/Ne$ feed line upstream of the volume loop. To initiate

Table 3
Experimental conditions and average kinetic data

Exp. No.	Catalyst sample	Feed flow rate (ml/min)[a]				Effluent H_2:CO	CO conversion (%)	CO conversion rate (μmol/g metal min^{-1})	Selectivity (%)		C_{5+} alpha[b]	N_{CO}/N_{Co}	k_{CO} (1/s)	N_{C*}/N_{CO}	k_{C*} (1/s)
		H_2	CO	Ne	Total				CH_4	C_{5+}					
1	Co-powder-1	12.0	6.0	6.0	24.0	1.86	8.6	60	14.8	67.6	0.77	0.0010	0.059	0.485	0.121
2	Si-Co21-1	20.0	10.0	10.0	40.0	1.80	16.0	2622	14.0	75.0	0.81	0.0291	0.088	0.308	0.287
3	Ti-Co6-1	8.0	4.0	4.0	16.0	1.83	8.4	2256	11.1	80.0	0.83	0.0228	0.097	0.563	0.173
4	Ti-Co6-2	10.0	5.0	5.0	20.0	1.82	12.5	2279	11.3	79.5	0.83	0.0221	0.101	0.531	0.191
5	Ti-Co14-1	23.0	11.5	11.5	46.0	1.83	12.9	2666	15.3	72.2	0.79	0.0335	0.078	0.346	0.226
6	CeMg-Co18-2	10.0	5.0	5.0	20.0	1.88	3.8	92	9.3	74.1	0.80	0.0435	0.002	0.069	0.030
7	Si-Co10-Re0.8-2	8.0	4.0	4.0	16.0	1.82	10.8	5770	13.6	77.2	0.82	0.0792	0.072	0.490	0.146
8	Si-Co20-Re1.7-1	16.9	8.5	8.5	33.9	1.82	13.2	5879	14.4	75.9	0.81	0.0535	0.108	0.531	0.203
9	Si-Co30-Re2.5-1	16.9	8.5	8.5	33.9	1.81	13.9	3990	16.5	72.1	0.79	0.0459	0.085	0.311	0.275
10	Si-Co30-Re2.5-2	16.9	8.5	8.5	33.9	1.79	11.0	3143	16.6	72.3	0.79	0.0401	0.077	0.328	0.235
11	Si-Co30-Re2.5-3	16.9	8.5	8.5	33.9	1.80	13.4	3850	15.7	73.3	0.80	0.0436	0.087	0.362	0.240
12	Ti-Co11-Re0.9-1	20.0	10.0	10.0	40.0	1.86	12.7	3167	14.7	73.2	0.80	0.0410	0.076	0.416	0.183
13	Ti-Co12-Re1.2-1	8.0	4.0	4.0	16.0	1.83	14.6	1018	13.9	74.0	0.80	0.0255	0.039	0.507	0.077
14	Ti-Co18-Re0.6-1	16.9	8.5	8.5	33.9	1.84	16.5	4042	12.9	76.7	0.82	0.0405	0.098	0.442	0.222
15	Al-Co12-Re1.0-2	16.9	8.5	8.5	33.9	1.81	13.4	4028	13.3	75.6	0.81	0.0563	0.070	0.428	0.164
16	Al-Co12-Re1.0-3	16.9	8.5	8.5	33.9	1.81	14.3	4301	11.9	78.0	0.82	0.0543	0.078	0.483	0.161
17	Al-Co20-Re2.2-3	20.0	10.0	10.0	40.0	1.81	16.1	3664	13.1	75.4	0.81	0.0545	0.066	0.527	0.125
18	Al-Co20-Re2.2-4	20.0	10.0	10.0	40.0	1.80	16.2	3711	13.3	74.8	0.81	0.0527	0.069	0.537	0.129
19	YAl-Co20-Re1.4-2	16.9	8.5	8.5	33.9	1.79	12.0	1769	11.3	74.4	0.80	0.0383	0.045	0.568	0.080
20	YSiAl-Co36-Re3.0-1	12.0	6.0	6.0	24.0	1.80	9.2	1596	12.5	73.6	0.80	0.0358	0.044	0.505	0.087
21	YSiAl-Co36-Re3.0-2	12.0	6.0	6.0	24.0	1.80	10.1	1743	12.6	73.9	0.80	NA	NA	NA	NA
22	ZnSiAl-Co36-Re3.0-1	10.0	5.0	5.0	20.0	1.79	1.2	169	8.1	82.6	NA	NA	NA	NA	NA
23	ZnSiAl-Co36-Re3.0-2	10.0	5.0	5.0	20.0	1.82	2.3	324	8.6	82.5	NA	0.0284	0.011	0.553	0.020
24	ZnSiAl-Co36-Re3.0-3	10.0	5.0	5.0	20.0	1.84	3.1	175	14.8	66.9	0.77	0.0229	0.007	0.453	0.017
25	MgSi-Co36-Re3.0-2	12.0	6.0	6.0	24.0	1.80	9.7	1134	11.0	73.1	0.80	0.0410	0.027	0.405	0.067
26	MgSi-Co36-Re3.0-3	12.0	6.0	6.0	24.0	1.81	7.7	907	11.7	65.7	0.76	0.0386	0.023	0.397	0.058
27	Ti-Re2.8-1	10.0	5.0	5.0	20.0	1.80	< 1	< 375	NA	NA	NA	0.51	< 0.002	NA	NA
28	Ti-Co11-Re0.9-2	20.0	10.0	10.0	40.0	2.03	10.3	2518	15.1	73.3	0.80	0.0410	0.060	0.305	0.198
29	Al-Co20-Re2.2-5	25.0	12.5	12.5	50.0	2.03	9.5	2830	15.3	72.8	0.80	0.0511	0.054	0.351	0.155

Reaction conditions, 221 °C, 5.5 atm (total, gauge); CO conversion and selectivity: average from 6 to 8 balances; Transient kinetic values: averages from 3 to 4 transients; CO_2 selectivity: $< 1\%$ in all tests.

[a] Standard temperature and pressure: 21.1 °C (70 °F), 1 atm.

[b] Anderson–Schulz–Flory alpha, based on C_{5+}/C_4 ratio.

an isotope transient, the volume loop valve was switched, sending the labeled ^{13}CO to the reactor. The inert, nonadsorbing Ne and Ar tracers provided a measure of the gas phase hold up in the reactor system. Most of the experiments were finished after the catalyst was on stream for approximately 1 day. The reported data, therefore, represent fresh catalytic activity. Since the activity measurements and the isotope transient experiments were performed sequentially on the same catalyst sample at the same reaction condition, the in situ site counts and surface inventories directly relate to the activity and selectivity data.

In order to reduce noise in our data, we performed multiple sampling for all data acquisitions. Thus, reported CO conversion and CH_4 selectivity data are based on 6 to 8 mass balances, while the transient kinetic values are averages of 3 to 4 transients. As a result of tight reaction control and careful data acquisition and analysis, repeated runs yielded good reproducibility (see, for example, experiments 9–11 in Table 3).

2.5. Kinetic analysis

On-line GC-MS was used to measure the Fischer–Tropsch activity and selectivity of the catalyst samples. In our measurements the following m/e ratios were used: CO, 12 and 28; Ne, 20 and 22; H_2, 2; CH_4, 16; and CO_2, 44. CO conversion values were determined by GC-MS from mass balances based on a premixed Ne internal standard. We observed a constant CO/Ne ratio during calibrations with different dilution levels and H_2/CO ratios, thus showing that sample discrimination did not occur in our GC-MS analyses. The FID signal of the GC provided the C_1–C_4 and C_1–C_7 production rates for Units T and C, respectively (the GC on Unit C was capable of separating C_1 to C_{22} hydrocarbons; however, only the C_1 to C_7 fraction was considered to be free of condensation problems). Selectivity to internal olefins, branched hydrocarbons, and oxygenates was very low, and thus ignored in our analyses.

2.6. Isotope transient analysis

Steady state isotope transient kinetic experiments provide the ideal in situ probe for cobalt FT catalysts [11–13,33–41]. The technique involves transient introduction of isotopic labels on reacting molecules and monitoring the labels in a time-resolved manner as they are incorporated into reaction products. The transient responses yield in situ information about the number and size of reactive intermediate pools on the catalyst, their lifetimes, and the sequence of reaction steps, all without disturbing the steady-state reaction. Thus, by providing an in situ probe of the steady-state catalytic processes, isotope transients can immediately distinguish changes in the number of sites from changes in site activity. The applications, experimental techniques, and data analysis of isotope transient kinetic experiments have been reviewed in several recent publications [42–47], and thus will not be described in detail.

We employed $^{12}CO/H_2/Ne \rightarrow {}^{13}CO/H_2/Ar$ (both with $1/2/1$ molar ratios) isotope switches at reaction steady state to investigate the active carbon pathways on the cobalt surface during FT synthesis. On-line MS monitored the progress of the isotope transients by using the following m/e ratios: ^{12}CO, 28 and 30; ^{13}CO, 29 and 31 (the ^{13}CO used in Unit T also contained $\sim 10\%$ ^{18}O), $^{12}CH_4$, 15 (contributions to m/e 15 from C_{2+} hydrocarbons were negligible compared to CH_4), Ne, 22; and Ar, 40. Sample transients in Unit T and C are shown in Figs. 3 and 4, respectively. Upon integration, the area bounded by the ^{12}CO and Ne tracer decay curves (see Figs. 3 and 4) yields t_{CO}, which is a measure (in seconds of CO flow) of the amount of CO reversibly adsorbed on the cobalt metal. To convert t_{CO} into the molar amount of reversibly adsorbed CO on the catalyst surface (N_{CO}), the following equation was used,

$$N_{CO} = \left[t_{CO} F_{CO} (1 - 0.5 f_{CO})\right], \tag{2}$$

where F_{CO} is the molar flow rate of CO in the feed and f_{CO} is the fractional CO conversion. From N_{CO}, the fraction of Co surface sites, N_{CO}/N_{Co}, can be readily obtained,

$$N_{CO}/N_{Co} = N_{CO}/[m_{Co}/AW_{Co}], \tag{3}$$

where m_{Co} is the mass of cobalt in the catalyst charge and AW_{Co} is the atomic weight of cobalt.

In our experiments, and in other experiments over a wider range of conditions and pressures, the amount of reversibly adsorbed CO was observed to be virtually saturated and constant. Thus, as noted earlier, we equated the number of active cobalt sites to N_{CO} with the assumption that N_{CO} is proportional to the number of active sites. The isotope transients thus provided an in situ measure of the number of available cobalt sites despite uncertainties regarding adsorption site requirements [48]. N_{CO}/N_{Co}, in turn, was used to calculate the CO turnover frequency, k_{CO}, in mol CO/(mol Co site s),

$$k_{CO} = -r_{CO} AW_{Co}/(N_{CO}/N_{Co}), \tag{4}$$

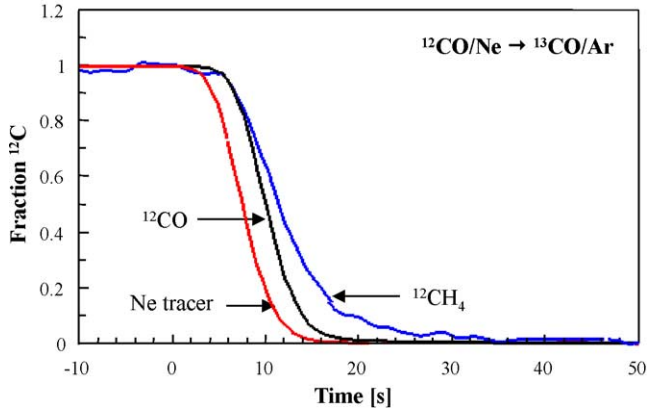

Fig. 3. Forward isotope transient in Unit T with 20.9 wt% Co on SiO_2. Reaction conditions: 221 °C, 6.5 atm of $H_2/CO/Ne = 2/1/1$.

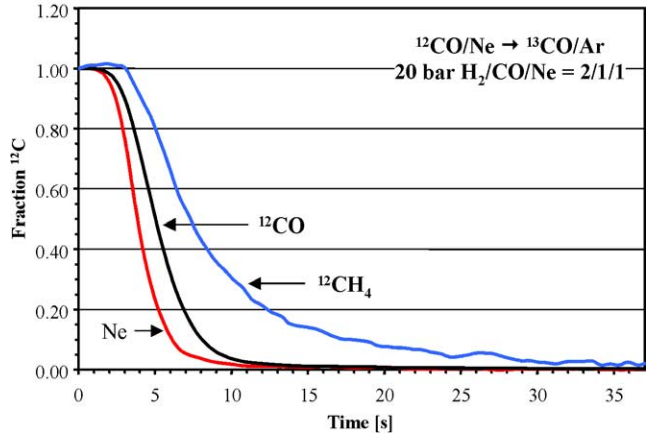

Fig. 4. Forward transient in Unit C with the 11 wt% Co–0.9 wt% Re on TiO_2 catalyst. Reaction conditions: 221 °C, 21 atm of $H_2/CO/Ne = 2/1/1$.

where r_{CO} is the rate of CO consumption in mol CO/(g Co s).

The isotopic response in CH_4 provides the amount and the residence time of the active carbon intermediates leading to CH_4 formation. Thus, integrating the area bounded by the $^{12}CH_4$ and Ne tracer decay curves (cf. Figs. 3 and 4) yields the residence time for the active carbon reporting as methane (τ_{CH_4}). Part of the surface ^{12}C measured in the $^{12}CH_4$ response originates from gas phase ^{12}CO after the isotope switch (the chromatographic effect for CO). In order to remove this artifact, we corrected τ_{CH_4} as follows:

$$\tau_{CH_4,\ \text{corrected}} = \tau_{CH_4} - 0.5 t_{CO}. \tag{5}$$

Consistent with other studies [11,12,33,35–37,40,41] and as evidenced by Figs. 3 and 4, the CH_4 transients observed in the current study can be reasonably represented by a single exponential, characterized by a single τ_{CH_4} value. Therefore, the reactivity of the active carbon intermediate pool leading to CH_4, $k_{C^*(CH_4)}$, can be simply expressed as the inverse of $\tau_{CH_4,\ \text{corrected}}$:

$$k_{C^*(CH_4)} = 1/\tau_{CH_4,\ \text{corrected}}. \tag{6}$$

Previous isotope transient studies of cobalt FT synthesis [33,39,40] have shown that the time dependence of the decay of ^{12}C in the higher hydrocarbons is equivalent to that of CH_4 and concluded that all hydrocarbon products arise virtually instantaneously from a common pool of carbon monomers. Thus, we can make the following assumption,

$$k_{C^*} = k_{C^*(CH_4)}, \tag{7}$$

where k_{C^*} is the reactivity of the carbon monomer pool leading to all hydrocarbon products. It follows from the above argument that the kinetics of C^* removal could have been measured in any of the products. Methane, however, is preferred, since it is easily measured by mass spectrometry. It is also the least susceptible of the hydrocarbon products to further holdup in the reactor due to mass transport, high solubility in the resident liquid product, or readsorption onto the catalyst surface. Since at steady state the rates of CO and active carbon conversion are equal, the following equation can be used to calculate the cobalt site coverage by the carbon monomer, N_{C^*}/N_{CO}:

$$N_{C^*}/N_{CO} = k_{CO}/k_{C^*} = \left[-r_{CO} A W_{Co}/(N_{CO}/N_{Co})\right]/k_{C^*}. \tag{8}$$

It should be noted that although CO_2 does not originate from the carbon monomer pool [49], we did not subtract the CO_2 production rate from the CO conversion rate, since the selectivity for CO_2 was always less than 1%; thus, the CO converted to CO_2 was negligible.

In order to determine if observed differences in the calculated turnover frequency and methane selectivity values are statistically significant, error bars were calculated based on the propagation of error that occurred in a single measurement. Typical errors for the GC-MS peak areas (CO, Ne, and CH_4) were $< 0.5\%$. The CO mass flow controller had a 1% full scale error, while the errors for determining t_{CO} and τ_{CH_4} from integration of the isotope transient curves had minimum–maximum error ranges of 3.3–14.6% (8.5% average) and 2.7–11.8% (6.6% average), respectively.

3. Results and discussions

Table 3 contains the results of the isotope transient experiments on the catalysts listed in Tables 1 and 2. In the following sections we discuss these results as they relate to the role of rhenium and support on the intrinsic site reactivity.

3.1. Effect of rhenium

As discussed earlier, our site activity measurements rely on a combination of mass balance and in situ site titration by CO. If exposed Re is present as surface segregated Re or as a separate phase on the support in a working Co–Re catalyst, it could modify the apparent site activity by contributing to the measured CO/C^* inventory and CO conversion. It is therefore important to understand the behavior of Re at our measurement conditions in order to correctly interpret the results for the Co–Re catalysts. To address this issue, we tested a 2.8 wt% Re/TiO_2 catalyst (sample 18 in Table 1) under the same conditions as applied in all other experiments in this study: 221 °C, 5.5 atm (gauge), $H_2/CO/Ne = 2/1/1$. The kinetic results for the Re/TiO_2 catalyst are depicted in Table 3 (entry 27). These results represent the catalyst performance after 80 h on stream, where Re dispersion, and with it catalytic activity, have dropped to 50% of the fresh values. Fresh N_{CO}/N_{Re} was ~ 1.0, which agrees well with the measured H_2 chemisorption value of 0.82 [50]. The average particle size (1.23 nm) in the fresh catalyst obtained by transmission electron microscopic analysis also indicates highly dispersed Re [51].

As indicated in Table 3, the activity of the catalyst was so low after 80 h on stream that we were unable to accurately measure CO conversion at the lowest space velocity allowed by the combination of our flow controllers and the catalyst capacity of our reactor. Based on the resolution of our measurements, we can put an upper limit of 1% on CO conversion. This represents a maximum possible turnover frequency value of 0.002 s^{-1}. A minimum value of the CO conversion rate was obtained from the measured C1–C4 production rates, ignoring the unmeasured C5+ products. The CO turnover frequency value of ~ 0.0001 s^{-1} calculated from the C1–C4 production rate, therefore, can be used as a minimum limit. A comparison of these values to the turnover frequencies measured under identical conditions (except for CO conversion that could not be matched) for Co/TiO_2 catalysts (see entries 3–5 in Table 3) indicates approximately two orders of magnitude lower activity for Re compared to Co. The implication of this finding is that the apparent site activity of a Re-promoted cobalt catalyst would be lower than that of a Co-only catalyst if Re was segregated onto the metal particle surface (site blockage) or if a separate Re phase was present (low activity sites). Unfortunately, due to the uncertainty in the CO conversion values for the Re catalyst, we cannot comment on the methane selectivity of Re/TiO_2.

We now consider the site-activity and methane selectivity effects of rhenium promotion by comparing the results obtained with Re-promoted and Co-only catalysts. The measured turnover frequency and methane selectivity values for Co and Co–Re catalysts supported on silica and titania are depicted in Figs. 5 and 6, respectively. The turnover frequency and methane selectivity values vary somewhat with both the silica- and the titania-supported catalysts. Although these variations are beyond the error in our experimental data (see error bars in Figs. 5 and 6), they do not correlate with the presence or absence of Re: the variation within the Co and Co–Re groups are the same as between the Co and the Co–Re samples. Note that the variations in site activity and methane selectivity also do not correlate with particle size (metal dispersion). This is not surprising, since the N_{CO}/N_{Co} values fall in a relatively narrow range of 2–5% minimizing any potential particle size effect. It is also worth pointing out that the well-known [17] dispersion aiding ef-

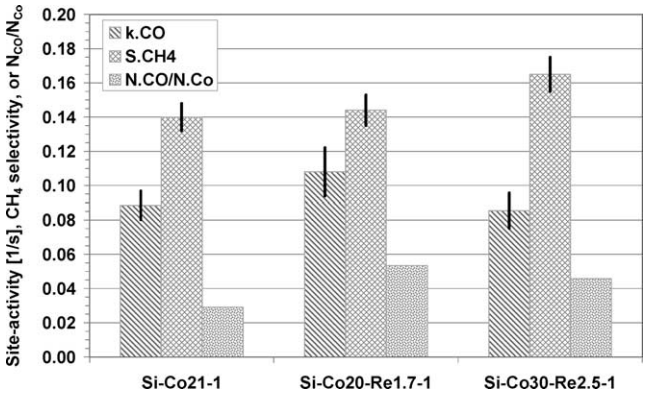

Fig. 5. The effect of Re on site activity, methane selectivity, and rapidly exchanging CO inventory with silica-supported Co catalysts in Fischer–Tropsch synthesis at 221 °C with 6.5 atm of $H_2/CO/Ne = 2{:}1{:}1$.

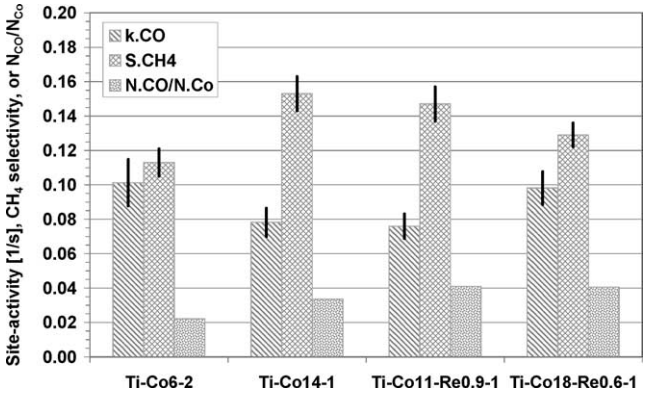

Fig. 6. The effect of Re on site activity, methane selectivity, and rapidly exchanging CO inventory with titania-supported Co catalysts in Fischer–Tropsch synthesis at 221 °C with 6.5 atm of $H_2/CO/Ne = 2{:}1{:}1$.

fect of Re is clearly noticeable: the Re-containing samples consistently show higher dispersion values (N_{CO}/N_{Co}) than that of the Co-only catalysts. These results are in agreement with earlier reports suggesting that Re does not affect the site activity [1,10,17,18] or selectivity [20] of cobalt Fisher–Tropsch catalysts. Guczi et al. [15] observed both an increase and a decrease in methane selectivity upon Re addition to Co supported on NaY or silica prepared by the sol/gel method. Although the authors have correlated the selectivity changes with the addition of Re, other factors such as gas composition variations or mass-transfer limitations might have also influenced the observed selectivity changes.

While the turnover frequency and methane selectivity are related to the overall CO conversion process, changes in the active carbon inventory (N_{C^*}/N_{CO}) and its turnover rate (k_{C^*}) can reveal if Re influences the balance of intermediates and their conversion rates in the Fischer–Tropsch conversion mechanism. We found previously [13], for example, that water reversibly increases the active carbon inventory by accelerating the dissociation of CO without increasing the reactivity of the downstream synthesis steps. This buildup of active carbon intermediates in turn explained the experimentally observed reduced methane selectivity upon an increase

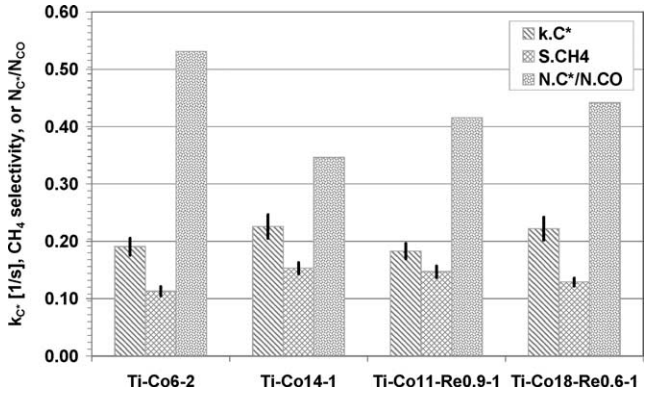

Fig. 7. The effect of Re on active carbon inventory, methane selectivity, and active carbon reactivity with titania-supported Co catalysts in Fischer–Tropsch synthesis at 221 °C with 6.5 atm of $H_2/CO/Ne = 2{:}1{:}1$.

in steam partial pressure. A similar analysis of our current data shows no correlation between the surface inventory or reactivity of active carbon intermediates and the presence or absence of Re. For example, Fig. 7 shows the experimental data for our TiO_2-supported catalysts tested. Just as in the case of CO turnover frequency and methane selectivity, the changes in the active carbon inventory and reactivity are just as large within the Co-only and Co–Re groups as the ones between the Co-only and the Co–Re catalysts. The variations are, again, larger than the experimental error, but their source is unknown. Fig. 7 also displays the methane selectivity data to show that, similar to water addition [13], increased active carbon inventory correlates with lower methane selectivity.

In summary, although all measured parameters (N_{CO}/N_{Co}, k_{CO}, S_{CH_4}, N_{C^*}/N_{CO}, k_{C^*}) showed variations larger than the experimental error, we found no evidence that Re influences site activity, selectivity, or the balance of reaction intermediates in cobalt-catalyzed Fischer–Tropsch synthesis. This observation is in agreement with earlier reports [1,10,17,18,20]. The very different reactivity of Re supports the notion of cobalt surface enrichment in metallic Co–Re alloys [17].

3.2. Effect of support

We selected an array of Re-promoted cobalt catalysts to study the effect of support. In the previous section we established that Re does not influence the rate and selectivity of the cobalt-catalyzed hydrocarbon synthesis process, thus, the conclusions from our study are expected to be also valid for unpromoted cobalt catalysts. As mentioned earlier, the sample suite included the three commonly available oxide supports, silica, alumina, and titania, as base cases. These commercially available supports are often modified by, for example, Group II, III, or IV oxide coatings considered to be activity and/or selectivity promoters or act as stabilizers. Thus, in order to investigate the effect of these oxide promoters, we also tested ceria-, yttria-, magnesia-, and ZnO-promoted Co–Re catalysts.

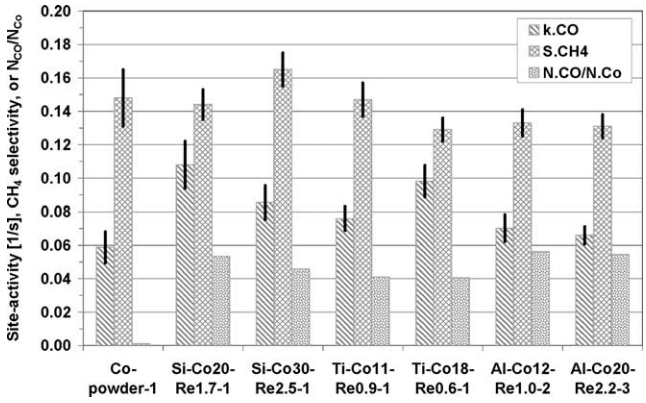

Fig. 8. The effect of support on site activity, methane selectivity, and rapidly exchanging CO inventory with Co catalysts in Fischer–Tropsch synthesis at 221 °C with 6.5 atm of $H_2/CO/Ne = 2{:}1{:}1$.

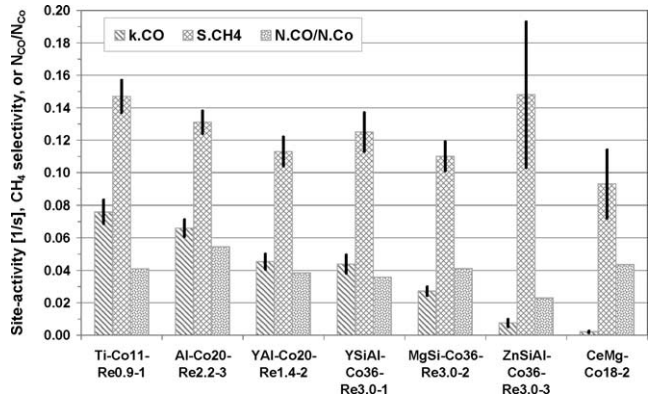

Fig. 9. The effect of support modification on site activity, methane selectivity, and rapidly exchanging CO inventory with Co catalysts in Fischer–Tropsch synthesis at 221 °C with 6.5 atm of $H_2/CO/Ne = 2{:}1{:}1$.

Fig. 8 compares the site activity, methane selectivity, and dispersion of unsupported Co and Co supported on SiO_2, TiO_2, and Al_2O_3. The lowest site activity was measured with the unsupported cobalt sample, which is likely the result of impurities that are difficult to eliminate during preparation and can easily affect a low surface area metal by diffusing to the surface. In fact, we had to prepare several samples before acceptable activities were attained with cobalt powders. With that caveat, from Fig. 8 we conclude that, while the variability of the site-activity and methane selectivity results is reproducible (cf. Experimental) and larger than the experimental error, it does not correlate with the presence, or absence, or with the bulk composition of the support. Apparently, the surface cobalt atoms of the relatively large (> 10 nm) cobalt particles present in our samples (and in typical supported Co Fischer–Tropsch catalysts [1–6]) are unaffected by the underlying support. This conclusion is in agreement with the results from earlier studies [1–6,10] and further builds the case for the structure and support insensitivity of cobalt-catalyzed Fischer–Tropsch synthesis. While we agree that the evidence by now for structure and support insensitivity is convincing, we will show that there are factors (albeit, so far unknown) that can substantially alter (in our examples always reduce) the site activity of cobalt (vide infra). The real (and as yet unexplained) variability in the site activity shows clearly the danger in using a single pair of experiments (even with tightly controlled reactions) to test the effects of support (or Re).

Supports are often modified in an attempt to improve catalyst activity, selectivity, or stability. In the Fischer–Tropsch synthesis, rare earth oxides have been reported to improve catalyst activity [10,11,52–55], selectivity [11,52–55], or stability [10] often by weakening metal support interaction and thus improving the reducibility of cobalt or creating special sites at the metal–support interface. The range of possible support modifiers and their combinations is virtually infinite. We chose a few modifiers as examples. These, listed in Table 1, include yttria as a rare earth modifier, other irreducible oxide modifiers, such as ZnO and magnesia, and a coprecipitated cobalt catalyst with a ceria–magnesia oxide component.

The site-activity and methane selectivity results for the support-modified catalysts are shown in Fig. 9 along with the results for two base case catalysts (leftmost bars in the figure). Interestingly, unlike the addition of Re, or the use of different unmodified supports, the site-activity values of all support-modified samples are significantly lower than those of the base case catalysts. Note that the metal dispersions are comparable to that of the base case catalysts thus Co particle size effects are not responsible for these changes. Since metal loadings are also comparable (in fact, somewhat higher), the sites should not have been impacted to a greater extent by potential impurities from reagents used in preparation than for the base case samples. While site activity is up to an order of magnitude lower, methane selectivity is not impacted. We have performed bulk chemical analysis of these samples, but could not find any of the known inhibitors/poisons, such as alkali metals, halogens, or sulfur. The activity of some of these samples was so low that we had to repeat experiments several times (increasing the catalyst charge) in order to get to or at least near the target conversion (see Table 2, experiments 6 and 24). Both metal site and pore blockage can be excluded since both the rapidly exchanged CO inventory and CH_4 selectivity values and transients are normal. We would expect a drop in CO inventory if metal sites were covered by some support components. Pore blockage, on the other hand, would substantially increase methane selectivity due to transport limitations [5]. Our results with yttria are somewhat surprising in light of earlier publications [10,11,52–55] documenting enhanced activity and/or selectivity upon rare earth modifications of silica or alumina supports. The lower than normal CO turnover frequency values with basic support modifiers, however, are in agreement with results previously reported for $Co/MgO \cdot SiO_2$ [55] and Co/MgO [56]. We were unable to find any fact-based explanation for the unusually low site activities of these catalysts; thus, we suspect that some low-level impurities that have high affinity to the metal surface but cannot be readily iden-

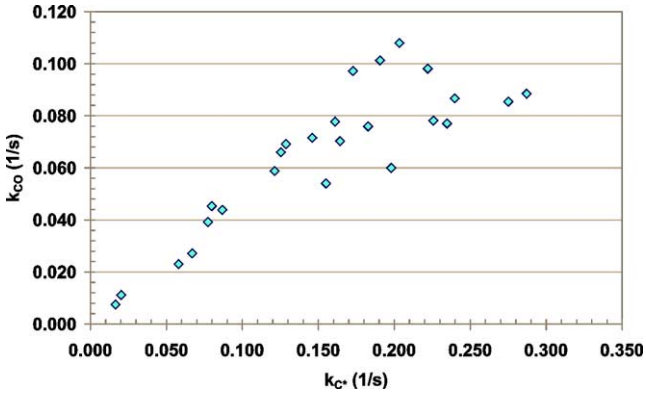

Fig. 10. CO turnover frequency versus active carbon reactivity in Co-catalyzed Fischer–Tropsch synthesis at 221 °C with 6.5 atm of H_2/CO/Ne = 2:1:1.

tified by bulk analysis are responsible for the observed rate inhibition. Although this issue certainly warrants further investigation, it is beyond the scope of the current study.

The data in Table 3 indicate that the support-modified catalysts with substantially reduced site activity (CO turnover frequency) also showed substantial and parallel changes in the carbon reactivity, k_{C^*}. As depicted in Fig. 10, the overall site activity correlates well with the reactivity of the active surface carbon intermediates for the entire suite of catalysts. Although there is increasing scatter at higher site-activity values, it seems that the lower site activity observed for the support-modified catalysts is also manifested in reduced surface carbon reactivity. Unlike the CO turnover frequency, the carbon reactivity changes cannot be attributed to extraneous adsorbed CO. This result suggests chemical modification (as opposed to some sort of physical blockage) of the active cobalt surface. Alkali metals are known to affect Fischer–Tropsch catalysts via this mechanism [57]; however, the bulk analysis of our samples did not find unusual levels of alkali metals.

3.3. Effect of active carbon coverage on selectivity

In our earlier studies [13,58,59], we have been able to discern a connection between methane selectivity and the active carbon inventory on the catalyst. In a study of the effect of water on the activity and selectivity of Co catalysts [13], for example, we found that reduced methane selectivity upon water cofeeding correlated with increased active carbon inventory. In a preliminary examination of some of the results of the current study, we were able to predict such a correlation [58,59]. The argument is based on the simple CO conversion model shown in Fig. 11, and the expectation that higher hydrocarbon growth would become more probable relative to methane formation with a higher active carbon coverage (for more detail see Ref. [13]). Fig. 12 displays the corresponding data obtained in the current investigation. It can be seen that despite substantial scattering of the data, a general trend of lower methane selectivity at increased active carbon inventory is recognizable. Thus, the variation

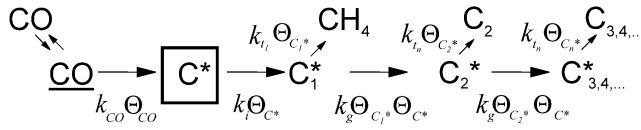

Fig. 11. Expanded version of the simple kinetic model depicting the paths to CH_4 and C_{2+} hydrocarbons [13].

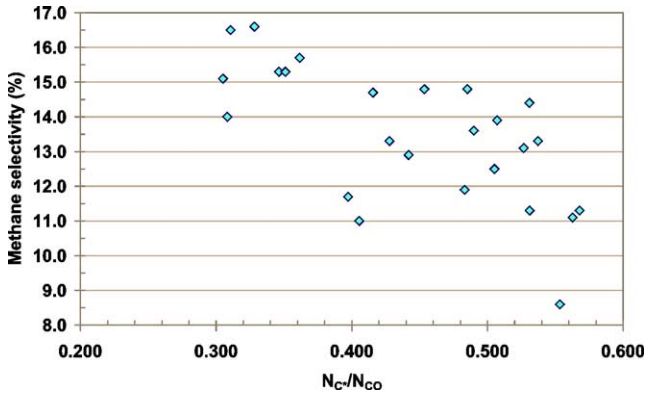

Fig. 12. Methane selectivity versus active carbon inventory in Co-catalyzed Fischer–Tropsch synthesis at 221 °C with 6.5 atm of H_2/CO/Ne = 2:1:1.

in methane selectivity seen in this study can be explained in part by changes in the active carbon inventory which result from nonidentical variations in CO and C* reactivity. Fischer–Tropsch selectivity is also influenced by factors other than "carbon crowding" (for example, the ones that govern H_2 activation), and these factors are responsible for the remaining scatter (outside experimental error). Other factors are clearly dominant for the ceria–magnesia-supported catalyst (Experiment 6 in Table 3), which shows a markedly different behavior and falls outside the range in Fig. 12. On this catalyst, both k_{CO} and k_{C^*} are greatly suppressed with respect to the standard supports, but here, one of the lowest methane selectivities in this study is associated with the lowest C*/CO ratio.

4. Summary

Our current study investigated the effect of Re promoter and support on the selectivity and activity of Co-catalyzed Fischer–Tropsch synthesis. Earlier investigations often relied on measuring the overall activity and selectivity, or used ex situ site-counting methods for establishing site activity. These methods, however, cannot establish site activity or account for the changes in active sites during the testing. In order to alleviate these concerns, we used the in situ measured rapidly exchanging adsorbed CO for active site-counting that was then used to calculate the turnover frequency. We also quantified the active carbon inventory and reactivity, which in turn affords more detailed insight into the changes in the intermediate steps of the CO conversion process.

We found that although Re itself adsorbs CO and has some Fischer–Tropsch activity, it does not affect Co site activity or selectivity. This result is in line with other publications suggesting that noble metal promoters, while they do enhance the reducibility of Co precursors, do not alter the catalytic behavior of the active cobalt metal. The lack of influence is likely due to the notion that Co enriches on the surface of Co–Re alloys in their fully reduced metallic state.

Unlike with rhenium, the effect of the support seems to be more complex. While Co supported on frequently used, commercially available SiO_2, TiO_2, and Al_2O_3 supports is unaffected by the support, support modifiers such as yttria, magnesia, and ZnO reduced Co site activity without changing methane selectivity. The largest site-activity drop was observed with a coprecipitated catalyst containing a ceria–magnesia oxide component. The reason for this negative impact is not yet fully understood; thus further studies are warranted.

Although we were unable to identify the factors leading to the observed variations in site activity, it is clear that reduced site activity correlates with reduced reactivity of the active carbon intermediates. While this correlation is readily observable, the ratio of site activities for CO and active carbon varies somewhat. This variation causes some variability in the active carbon coverage and methane selectivity as predicted by our simple mechanistic model of Fischer–Tropsch synthesis. Since the observed changes clearly affect the internal balance of reaction rates and inventories of reaction intermediates, they are likely the result of a chemical modification of the active metal site by a yet unknown factor as opposed to physical site blockage.

Acknowledgment

The authors express their gratitude for the generous supply of catalyst samples by Drs. Claude C. Culross, Andre Malek, Charles H. Mauldin, John L. Robbins, Stuart L. Soled, and by Mr. Sabato Miseo; for the TEM characterization by Mrs. Chris E. Kliewer, and for the TGA and H_2 chemisorption analyses of selected samples by Dr. Stuart L. Soled and Mr. Joseph E. Baumgartner (all of ExxonMobil). The financial support of ExxonMobil Research and Engineering Co. is also gratefully acknowledged.

References

[1] E. Iglesia, Stud. Surf. Sci. Catal. 107 (1997) 153.
[2] E. Iglesia, Appl. Catal. A 161 (1997) 59.
[3] E. Iglesia, S.L. Soled, R.A. Fiato, G.H. Via, Stud. Surf. Sci. Catal. 81 (1994) 433.
[4] E. Iglesia, S.C. Reyes, R.J. Madon, S.L. Soled, Adv. Catal. 39 (1993) 221.
[5] E. Iglesia, S.C. Reyes, S.L. Soled, in: E.R. Becker, C.J. Pereira (Eds.), Computer-Aided Design of Catalysts, Dekker, New York, 1993, p. 199.
[6] E. Iglesia, S.L. Soled, R.A. Fiato, J. Catal. 137 (1992) 212.
[7] B.G. Johnson, C.H. Bartholomew, D.W. Goodman, J. Catal. 128 (1991) 231.
[8] J.J.C. Geerlings, M.C. Zonnevylle, C.P.M. De Groot, Surf. Sci. 241 (1991) 315.
[9] S.-W. Ho, M. Houalla, D.M. Hercules, J. Phys. Chem. 94 (1990) 6396.
[10] R. Oukaci, A.H. Singleton, J.G. Goodwin Jr., Appl. Catal. A 186 (1999) 129.
[11] F. Rohr, O.A. Lindvag, A. Holmen, E.A. Blekkan, Catal. Today 58 (2000) 247.
[12] K.F. Hanssen, E.A. Blekkan, D. Schanke, A. Holmen, Stud. Surf. Sci. Catal. 109 (1997) 193.
[13] C.J. Bertole, C.A. Mims, G. Kiss, J. Catal. 210 (2002) 84.
[14] A. Barbier, A. Tuel, I. Arcon, A. Kodre, G.A. Martin, J. Catal. 200 (2001) 106.
[15] L. Guczi, G. Stefler, Z. Schay, I. Kiricsi, F. Mizukami, M. Toba, S. Niwa, Stud. Surf. Sci. Catal. 130 (2000) 1097.
[16] R. Mauti, PhD thesis, Univ. of Toronto, 1994.
[17] C.H. Mauldin, D.E. Varnado, Surface Sci. Catal. 136 (2001) 417.
[18] S. Vada, A. Hoff, E. Adnanes, D. Schanke, A. Holmen, Top. Catal. 2 (1995) 155.
[19] G. Jacobs, T.K. Das, Y. Zhang, J. Li, G. Racoillet, B.H. Davis, Appl. Catal. A 233 (2002) 263.
[20] M. Ronning, D.G. Nicholson, A. Holmen, Catal. Lett. 72 (2001) 141.
[21] S. Sun, N. Tsubaki, K. Fujimoto, Chem. Lett. (2000) 176.
[22] J.G. Price, D. Glasser, D. Hildebrandt, N.J. Coville, Stud. Surf. Sci. Catal. 107 (1997) 243.
[23] A. Moen, D.G. Nicholson, Chem. Mater. 9 (1997) 1241.
[24] A.M. Hilmen, D. Schanke, A. Holmen, Catal. Lett. 38 (1996) 143.
[25] A. Kogelbauer, J.G. Goodwin Jr., R. Oukaci, J. Catal. 160 (1996) 125.
[26] F.B. Noronha, A. Frydman, D.A.G. Aranda, C. Perez, R.R. Soares, B. Morawek, D. Castner, C.T. Campbell, R. Frety, M. Schmal, Catal. Today 28 (1996) 147.
[27] L.A. Bruce, M. Hoang, A.E. Hughes, T.W. Turney, Stud. Surf. Sci. Catal. 81 (1994) 427.
[28] R. Oukaci, J.G. Goodwin Jr., G. Marcelin, A. Singleton, ACS Div. Fuel Chem. Preprints 39 (1994) 1117.
[29] A. Hoff, E.A. Blekkan, A. Holmen, D. Schanke, in: L. Guczi, et al. (Eds.), New Frontiers in Catalysis, Elsevier, New York, 1993, p. 2067.
[30] C.J. Kim, US patent 5,227,407, 1993.
[31] C.J. Kim, Europe patent 355,218, 1990.
[32] C.J. Kim, Europe patent 339,923, 1989.
[33] H.A.J. Van Dijk, J.H.B.J. Hoebink, J.C. Schouten, Chem. Eng. Sci. 56 (2001) 1211.
[34] M. Rothaemel, K.F. Hanssen, E.A. Blekkan, D. Schanke, A. Holmen, Catal. Today 40 (1998) 171.
[35] M. Rothaemel, K.F. Hanssen, E.A. Blekkan, D. Schanke, A. Holmen, Catal. Today 38 (1997) 79.
[36] A.R. Belambe, R. Oukaci, J.G. Goodwin Jr., J. Catal. 166 (1997) 8.
[37] K.R. Krishna, A.T. Bell, J. Catal. 139 (1993) 104.
[38] T. Komaya, A.T. Bell, J. Catal. 146 (1994) 237.
[39] C. Mims, J. Krajewski, K. Rose, M.T. Melchior, Catal. Lett. 7 (1990) 119.
[40] C.A. Mims, L.E. McCandlish, J. Phys. Chem. 91 (1987) 929.
[41] P. Biolen, J.N. Helle, F.G.A. van den Berg, W.M.H. Sachtler, J. Catal. 81 (1983) 450.
[42] S.C. Van der Linde, T.A. Nijhuis, F.H.M. Dekker, F. Kapteijn, J.A. Mouljin, Appl. Catal. A 151 (1997) 27.
[43] S.L. Shannon, J.G. Goodwin Jr., Appl. Catal. A 151 (1997) 3.
[44] A.M. Efstathiou, X.E. Verykios, Appl. Catal. A 151 (1997) 109.
[45] S.L. Shannon, J.G. Goodwin Jr., Chem. Rev. 95 (1995) 677.
[46] C. Mirodatos, Catal. Today 9 (1991) 83.
[47] C.A. Mims, R.B. Hall, A.J. Jacobson, J.T. Lewandowski, G. Meyers, in: F. Hoffman, D. Dwyer (Eds.), Surface Science of Catalysis: In-Situ Probes and Reaction Kinetics, in: ACS Symp. Series, Vol. 482, Amer. Chem. Society, Washington, 1991, p. 230.

[48] G.P. van der Laan, A.A.C.M. Beenackers, Catal. Rev.-Sci. Eng. 41 (1999) 255.
[49] H.A.J. Van Dijk, PhD thesis, Technische Universiteit Eindhoven, Holland, 2001.
[50] S.L. Soled, ExxonMobil Res. & Eng., private communication.
[51] C.E. Kliewer, ExxonMobil Res. & Eng., private communication.
[52] S. Ali, B. Chen, J.G. Goodwin Jr., J. Catal. 157 (1995) 35.
[53] S. Vada, A.M. Kazi, F.K. Bedu-Addo, B. Chen, J.G. Goodwin Jr., Stud. Surf. Sci. Catal. 81 (1994) 443.
[54] N. Takahashi, T. Mori, A. Miyamoto, T. Hattori, Y. Murakami, Appl. Catal. 38 (1988) 61.
[55] S. Halvorsen, K. Vinje, S. Lofthus, I.M. Dahl, Stud. Surf. Sci. Catal. 61 (1991) 281.
[56] R.C. Reuel, C.H. Bartholomew, J. Catal. 85 (1994) 78.
[57] E.A. Blekkan, A. Holmen, S. Vada, Acta Chem. Scand. 47 (1993) 275.
[58] C.J. Bertole, G. Kiss, C.A. Mims, in: 17th North Am. Cat. Soc. Mtg., Toronto, Ontario, Canada, Technical Program, 2001, p. 264.
[59] C.J. Bertole, C.A. Mims, Stud. Surf. Sci. Catal. 136 (2001) 375.